

Classifying Multipartite Continuous Variable Entanglement Structures through Data-augmented Neural Networks

Xiaoting Gao,^{1,*} Mingsheng Tian,^{1,*} Feng-Xiao Sun,^{1,2} Ya-Dong Wu,³ Yu Xiang,^{1,2,†} and Qiongyi He^{1,2,4,5,‡}

¹*State Key Laboratory for Mesoscopic Physics, School of Physics,
Frontiers Science Center for Nano-optoelectronics,*

& Collaborative Innovation Center of Quantum Matter, Peking University, Beijing 100871, China

²*Collaborative Innovation Center of Extreme Optics,
Shanxi University, Taiyuan, Shanxi 030006, China*

³*John Hopcroft Center for Computer Science, Shanghai Jiao Tong University, Shanghai, 200240, China*

⁴*Peking University Yangtze Delta Institute of Optoelectronics, Nantong, Jiangsu 226010, China*

⁵*Hefei National Laboratory, Hefei 230088, China*

Neural networks have emerged as a promising paradigm for quantum information processing, yet they confront the challenge of generating training datasets with sufficient size and rich diversity, which is particularly acute when dealing with multipartite quantum systems. For instance, in the task of classifying different structures of multipartite entanglement in continuous variable systems, it is necessary to simulate a large number of infinite-dimension state data that can cover as many types of non-Gaussian states as possible. Here, we develop a data-augmented neural network to complete this task with homodyne measurement data. A quantum data augmentation method based on classical data processing techniques and quantum physical principles is proposed to efficiently enhance the network performance. By testing on randomly generated tripartite and quadripartite states, we demonstrate that the network can indicate the entanglement structure among the various partitions and the accuracies are significantly improved with data augmentation. Our approach allows us to further extend the use of data-driven machine learning techniques to more complex tasks of learning quantum systems encoded in a large Hilbert space.

Introduction—Neural networks, as biologically inspired computing models, have achieved remarkable success in many domains including quantum physics. These models provide innovative solutions to complex problems such as quantum state reconstruction [1–3], learning quantum features [4–9], and even discovering new physics [10–13], demonstrating their powerful capabilities in the field. The effectiveness of these data-driven techniques, whether applied to classical or quantum problems, fundamentally depends on the quality of the underlying datasets [14–16]. As the size and diversity of training data increase, neural networks improve their ability to generalize to unseen cases. Usually, assembling such comprehensive datasets requires considerable time and resources for careful data collection and accurate annotation.

This becomes more challenging in dealing with multipartite quantum systems, constrained by the higher complexity as the number of subsystems increases. Multipartite entanglement, for instance, is classified according to the separability among all possible combinations of subsystems and plays an essential role in quantum physics [17–20]. However, for an arbitrary multipartite quantum state, classifying the entanglement structure in terms of different multipartitions with experimentally feasible measurements remains a daunting task.

Some efforts have been made to explore the potential of neural networks in the detection of multipartite entanglement structure in discrete variable systems [21–24], aiming to circumvent the high cost of full

quantum state tomography [25]. In continuous variable (CV) systems, where the Hilbert space is of infinite dimension [26], conventional tomography is even more impractical [27]. This problem becomes especially acute for non-Gaussian states, due to the existence of various complex high-order correlations. In this context, neural networks provide an experimentally feasible approach by analyzing statistics features extracted from homodyne measurements [4, 9]. However, the challenge of simulating sufficient infinite-dimension data containing different types of non-Gaussian states prevents direct application of such data-driven algorithms to multipartite CV cases. As the number of subsystems increases, this becomes an exceptionally hard problem.

The contributions of this work are twofold. First, we develop a neural network model capable of classifying the entanglement structures of arbitrary multipartite CV states using experimental-accessible homodyne measurement data. Second, to address the challenge in simulating multipartite CV systems, we propose a quantum data augmentation (QDA) method that significantly enhances the classification accuracy. The data augmentation operations are derived from both classical data processing techniques and quantum physical principles, such as entanglement invariance under mode permutation and the convexity of separable states. Inspired by the resource-preserving free operations in quantum resource theory [28], a wider range of label-preserving transformations can be designed to increase the volume and diversity of the training dataset

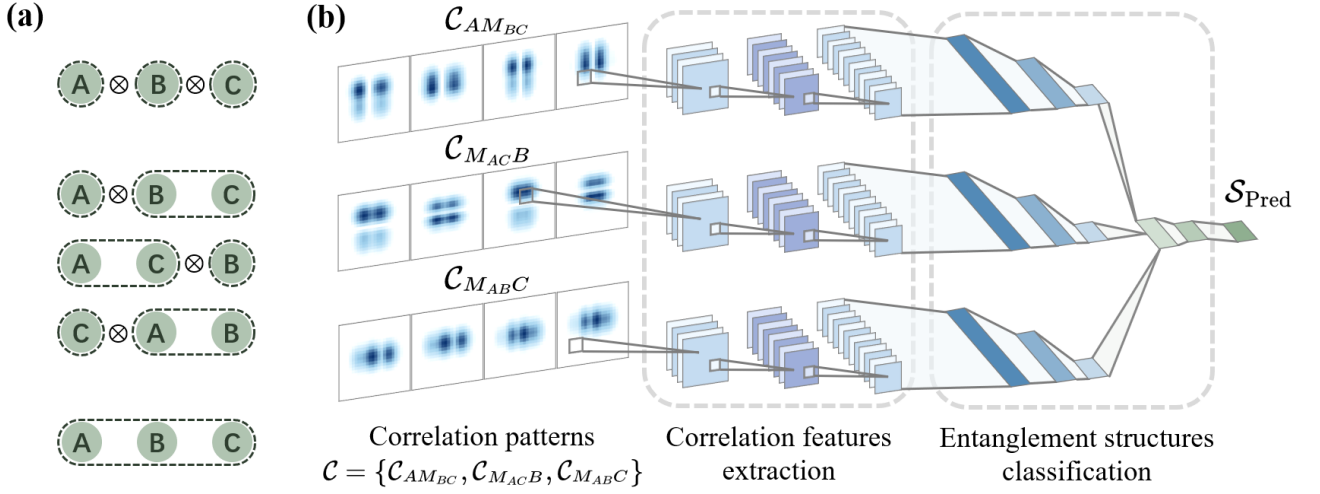


FIG. 1. (a) The tripartite entanglement structures for the partitions of fully separable partition $1 \otimes 1 \otimes 1$, three biseparable partitions $1 \otimes 2$, and fully inseparable states. (b) The neural network architecture for this task. Three groups of correlation patterns \mathcal{C}_{AMBC} , \mathcal{C}_{MACB} , and \mathcal{C}_{MABC} provide correlation features of $A - BC$, $B - AC$, and $C - AB$ splitting, respectively. Mode M_{ij} denotes an output mode from a beam splitter \hat{U}_{ij} mixing modes i and j . The features are extracted by convolutional layers and subsequently classified by fully connected layers into three classes of tripartite entanglement structures as shown in (a), resulting in a predicted entanglement structure label $\mathcal{S}_{\text{Pred}}$.

effectively.

We apply this data-augmented neural network for tripartite and quadripartite CV systems in all possible multi-partitions, including some typical multipartite non-Gaussian states. Compared to the accuracies of 0.929 and 0.762 using only original datasets, the network with QDA can remarkably improve them to 0.976 and 0.938 for the two cases. Therefore, our results provide a novel approach for classifying multipartite CV entanglement structures in an experimentally accessible way. Moreover, using the QDA method to efficiently generate training data, neural networks can be extended for broader tasks in detecting quantum resources of multipartite systems.

Multipartite entanglement structures— In a multipartite quantum system, entanglement detection goes beyond simply identifying the presence of entanglement; it also involves determining its detailed structure. Specifically, any $\mathcal{R}_1 | \dots | \mathcal{R}_j$ -separable state can be decomposed in the form $\hat{\rho} = \sum_{\gamma} p_{\gamma} \hat{\rho}_{\mathcal{R}_1}^{(\gamma)} \otimes \dots \otimes \hat{\rho}_{\mathcal{R}_j}^{(\gamma)}$, where \mathcal{R}_i describes an ensemble of modes and $\hat{\rho}_{\mathcal{R}_i}^{(\gamma)}$ denotes the reduced density matrix of $\hat{\rho}^{(\gamma)}$ on the subsystem \mathcal{R}_i [29]. In the following task, we classify cases with the same number of modes in each subsystem \mathcal{R}_i as the same multi-partition class and label them by \mathcal{S} . For example, states with separability $A|BC$, $B|AC$, and $C|AB$ all belong to the multi-partition class $\mathcal{S} = 1 \otimes 2$.

Training state set construction— We train the neural network on a broad set of random mixed CV states, including all Gaussian states and most experimentally

achievable non-Gaussian states. As illustrated in Fig. 1(a), we start with the simplest multipartite case: tripartite states. To collect balanced samples for all possible classes of states with different multi-partitions \mathcal{S} in a random way, we first generate a large number of m -mode ($m \leq 3$) seed states $\hat{\sigma}_m$. Then we use these seed states to separately construct each class. For examples, states with $\mathcal{S} = 1 \otimes 1 \otimes 1$ can be decomposed into a tensor product of three single-mode seed states $\otimes_{i=1}^3 \hat{\sigma}_1^{(i)}$, while states with $\mathcal{S} = 1 \otimes 2$ can be decomposed into a tensor product $\hat{\sigma}_1 \otimes \hat{\sigma}_2$ of a single-mode seed state $\hat{\sigma}_1$ and a two-mode entangled seed state $\hat{\sigma}_2$.

The seed states $\hat{\sigma}_m$ are generated based on a stellar formalism, which gives an operational characterization of non-Gaussian states [30–32]. This formalism is developed upon the stellar function $F_{\psi}^*(\mathbf{z}) \equiv e^{\frac{1}{2}\|\mathbf{z}\|^2} \langle \mathbf{z}^* | \psi \rangle$ of a normalised pure state $|\psi\rangle$, where $|\mathbf{z}\rangle$ is a coherent state with complex amplitude \mathbf{z} . The number of zeros of $F_{\psi}^*(\mathbf{z})$ defines the stellar rank r , which measures the non-Gaussianity of state $|\psi\rangle$. Consequently, all Gaussian states have $r = 0$ and all Gaussian unitaries preserve the stellar rank. Any m -mode pure state with finite stellar rank r can be decomposed into $\hat{G}|C(r)\rangle$, where \hat{G} is a general m -mode Gaussian unitary, consisting of squeezing, displacement, and beam splitters, and $|C(r)\rangle$ named as a core state [31], is an m -mode state with finite support over the Fock basis and stellar rank r . In our work, we focus on states with $r \leq 3$. To summarize, each m -mode seed state $\hat{\sigma}_m$ is obtained from a random core state $|C(r)\rangle$ with a given stellar rank r , followed by an m -mode Gaussian unitary with random parameters and m loss channels [33] with random efficiencies η

($l = 1, \dots, m$), given by

$$\hat{\sigma}_m = \left(\prod_{l=1}^m \hat{L}_l(\eta_l) \right) \hat{G} |C(r)\rangle \langle C(r)| \hat{G}^\dagger \left(\prod_{l=1}^m \hat{L}_l^\dagger(\eta_l) \right), \quad (1)$$

where each \hat{L}_l is a Kraus operator of the loss channel.

Following the definition of entanglement structure in terms of multi-partitions, entangled seed states are required as necessary components in the cases except for the fully separable partition. Furthermore, these entangled seed states must be fully inseparable to rule out any possible separability from seed states and avoid overlap between different multipartite separability classes. Here we adopt a recently proposed criterion based on quantum Fisher information to identify these fully inseparable seed states [34]. Additionally, mixtures within each product case are also considered. In the tripartite case, we construct a training dataset of 30 000 states, with 10 000 states for each class.

Correlation patterns from homodyne detection— Our aim is to map certain experimentally feasible correlation features, e.g., patterns extracted from homodyne detection, to multipartite entanglement structures described by different multi-partitions \mathcal{S} . Homodyne detection is a projective measurement on eigenstates of orthogonal quadrature operators $\hat{x}_l = (\hat{a}_l^\dagger + \hat{a}_l)$ and $\hat{p}_l = i(\hat{a}_l^\dagger - \hat{a}_l)$, where \hat{a}_l is the photon annihilation operator of mode $l \in \{A, B, C\}$ [27]. According to Born's rule, with $\hat{x}_l |X_l\rangle = X_l |X_l\rangle$, the probability of obtaining outcome (X_A, X_B, X_C) when simultaneously measuring \hat{x}_l on three modes of state $\hat{\rho}$ is given by $\mathcal{P}(X_A, X_B, X_C) \equiv \langle X_A; X_B; X_C | \hat{\rho} | X_A; X_B; X_C \rangle$. To ensure correlation features are not overlooked when only measuring reduced states, we use a balanced beam splitter $\hat{U}_{ij} = e^{\frac{\pi}{4}(\hat{a}_i^\dagger \hat{a}_j - \hat{a}_i \hat{a}_j^\dagger)}$ to mix modes i and j , producing two output modes M_{ij} and N_{ij} . By measuring one of the mixed modes M_{ij} and the remaining mode k yields two variable quadrature statistics, thereby extracting more pattern information with fewer measurements. As an example, by mixing modes B and C on a beam splitter \hat{U}_{BC} and then measuring quadrature X_A of mode A and quadrature $X_{M_{BC}}$ of the mixed mode M_{BC} , we obtain the joint probability given by

$$\begin{aligned} \mathcal{P}(X_A, X_{M_{BC}}) &= \langle X_A; X_B | \hat{U}_{BC} \hat{\rho} \hat{U}_{BC}^\dagger | X_A; X_B \rangle \\ &= \langle X_A; \frac{X_B + X_C}{\sqrt{2}} | \hat{\rho} | X_A; \frac{X_B + X_C}{\sqrt{2}} \rangle. \end{aligned} \quad (2)$$

Apart from $\mathcal{P}(X_A, X_{M_{BC}})$, we classically simulate other three joint probability distributions of $\mathcal{P}(X_A, P_{M_{BC}})$, $\mathcal{P}(P_A, X_{M_{BC}})$, and $\mathcal{P}(P_A, P_{M_{BC}})$ to capture correlation features between subsystems A and BC , which corresponds to one of the bipartitions we aim to detect. Considering the other two cases with respect to $B - AC$

and $C - AB$ splitting, we simulate a total of twelve joint probability distributions for each state (see Supplemental Material [35] for explicit expressions). To process them through the network, we bin every joint probability distribution into a 24×24 pixel grid, named a correlation pattern.

For each state $\hat{\rho}$, the twelve correlation patterns are denoted by $\mathcal{C} = \{\mathcal{C}_{AM_{BC}}, \mathcal{C}_{M_{AC}B}, \mathcal{C}_{M_{AB}C}\}$. These correlation patterns are fed into the neural network for training, together with the known multi-partitions \mathcal{S} . As shown in Fig. 1(b), the neural network is composed of three convolutional sub-networks [37], with each processing four correlation patterns to a vector. The three vectors are then combined through fully connected layers, and classified to a final outcome, i.e. the predicted multi-partitions $\mathcal{S}_{\text{Pred}}$. We hold 80% of the 30 000 simulated samples as an original training dataset.

Quantum data augmentation— During training, the performance of neural networks heavily depends on the size and diversity of training data. However, for a multipartite non-Gaussian system, the data complexity increases with the number of modes m and the stellar rank r [38], requiring a larger dataset to capture

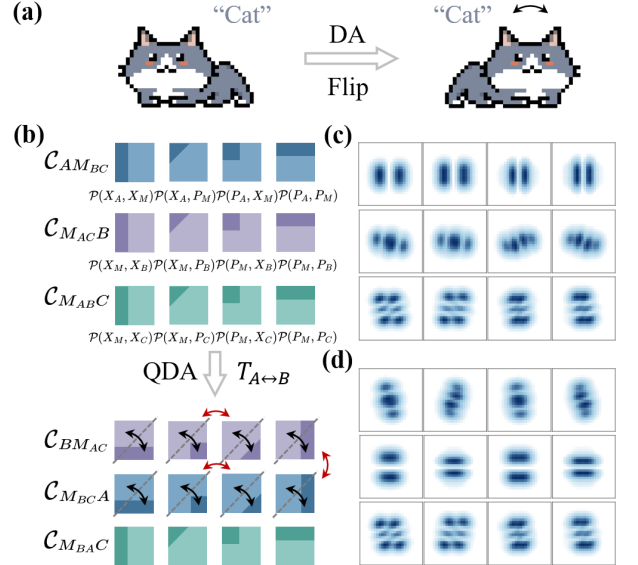


FIG. 2. (a) In a classical image classification task, data augmentation operations such as flipping can efficiently provide new samples beyond the original dataset, while the label “cat” remains invariant. (b) The schematic of how correlation patterns \mathcal{C} are transformed when modes A and B are swapped, while maintaining both the validity of transformed quantum measurement data and the invariance of multi-partitions label \mathcal{S} . Black arrows represent flipping along the dashed lines and red arrows represent exchanging the patterns. (c) Correlation patterns \mathcal{C} of an original $A|BC$ biseparable state $\hat{\rho}_{A|BC}$. (d) Rearrangement of \mathcal{C} through QDA, following the transformation $T_{A \leftrightarrow B}$ in (b), which efficiently provides a new sample to the dataset.

this growing diversity. Therefore, efficiently producing comprehensive training data for multipartite CV systems is central to addressing these machine learning problems. To solve this, we employ a technique called quantum data augmentation, originally developed in classical tasks to efficiently generate synthetic samples from an existing dataset, thereby enhancing the model’s performance [39].

The augmentation operations typically involve subtle variations that do not affect the model’s predictions. An example of classical data augmentation (DA) via image flipping is shown in Fig. 2(a), where a cat flipped horizontally remains a cat, preserving its label in an image classification task. Motivated by the success of DA in classical tasks, we introduce a QDA method and explore how augmented data can be constructed in the task of learning quantum systems. Similar to classical tasks, these augmentation operations preserve the labels of quantum states.

The first QDA operation is based on the mode permutation, denoted as T . Obviously, the entanglement structure is invariant with respect to the mode indexing, thus the label \mathcal{S} remains the same value when rearranging the three modes of state $\hat{\rho}$. An example of this QDA operation is given in Fig. 2(b). The mode permutation $T_{A \leftrightarrow B}$ can be easily achieved by flipping the pattern diagonally and then exchanging correlation patterns of the first two rows and the middle two columns. Figure 2(c) gives the simulated correlation patterns \mathcal{C} of a biseparable state $\hat{\rho}_{A|BC}$. The correlation patterns after performing $T_{A \leftrightarrow B}$ are shown in Fig. 2(d). This rearrangement keeps the invariance of the multipartitions label \mathcal{S} at $1 \otimes 2$, but makes it a new training sample for the neural network. In principle, for an m -mode quantum system, QDA based on mode permutation can expand the size of the dataset to $m!$ times its original size.

In addition to mode permutation, some quantum properties can also be utilized as QDA operations. For instance, in our task, a convex combination of any separable states remains separable [19], keeping the invariance of fully separable partition label $\mathcal{S} = 1 \otimes 1 \otimes 1$. Meanwhile, the correlation patterns of the convexly combined states can also be efficiently obtained, due to the linearity of the expectation value function. This QDA operation further enlarges the training dataset. Moreover, we find that the QDA method can remarkably alleviate the overfitting problem during training [40] and help the neural network converge to a much lower loss value [35].

Entanglement structures classification— By testing them on the rest 20% simulated samples, the classification performance of models trained with the original tripartite dataset and augmented datasets are assessed, respectively, as presented in Figs. 3(a) and (c). The accuracy measures the ratio of correctly predicted samples to the total number of samples in the test

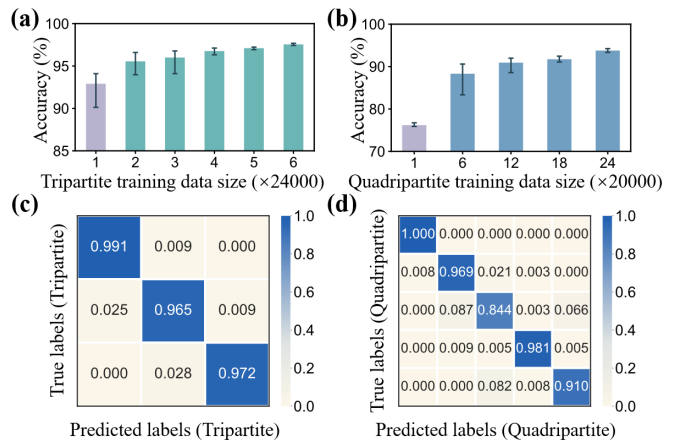


FIG. 3. (a, b) Testing accuracies for tripartite and quadripartite entanglement structure predictions using neural networks trained on the original datasets (24,000 samples for tripartite and 20,000 samples for quadripartite; purple bars) and on augmented datasets (green and blue bars, respectively). Error bars reflect variability across five repetitions. (c, d) Confusion matrices for tripartite and quadripartite entanglement structure predictions after QDA, with datasets enlarged by factors of 6 and 24, respectively. In (c), the diagonal elements (top-left to bottom-right) represent prediction accuracies for the tripartite partitions of $1 \otimes 1 \otimes 1$, $1 \otimes 2$, and fully inseparable classes. In (d), the diagonal elements represent accuracies for quadripartite partitions of $1 \otimes 1 \otimes 1 \otimes 1$, $1 \otimes 2 \otimes 1$, $2 \otimes 2$, $1 \otimes 3$, and fully inseparable classes, respectively.

dataset, that is, $N(\mathcal{S}_{\text{Pred}} = \mathcal{S})/N_{\text{total}}$. In Fig. 3(a), the achieved accuracy when only the original dataset is fed (purple bar) is 0.929. After using augmented data in multiples of the original dataset size, the green bars show significant improvements in the accuracies of entanglement structure prediction. It can be raised to 0.976, when the size of the augmented dataset expands to six times of the original size. A confusion matrix is also evaluated to demonstrate the ability of the neural network to distinguish among different multi-partitions, as depicted in Fig. 3(c). In this matrix, each row represents the samples of a true class and sums to 1, while each column represents the samples of a predicted class. Using our data-augmented neural network, the entanglement structure in terms of different multi-partitions can be detected with a prediction accuracy higher than 0.965 only based on limited homodyne measurement data.

The QDA method is further tested in the quadripartite entanglement structure classification task. For each quadripartite state, we mix three modes using two beam splitters, then sixteen correlation patterns are obtained by measuring the remaining mode and one of the outputs. See Supplemental Material for more details [35]. A neural network with a similar architecture to the tripartite case is trained with an original dataset containing 20 000

samples. These samples are evenly distributed across four classes of states, each representing a multi-partition class of fully separable partition $1 \otimes 1 \otimes 1 \otimes 1$, tri-separable partition $1 \otimes 2 \otimes 1$, biseparable partitions $2 \otimes 2$ and $1 \otimes 3$, and fully inseparable states. As shown in Fig. 3(b), the network trained with the original dataset only reaches an accuracy of around 0.762 on 5000 testing samples. After applying QDA, the augmented dataset becomes 24 times larger than the original one, significantly boosting the accuracy to 0.938, as depicted by the blue bars. Figure 3(d) shows the confusion matrix after enlarging the training dataset through the QDA method. Our data-augmented network can perfectly classify the fully separable states and achieves a high accuracy of 0.910 in identifying fully quadripartite inseparable states. Evidently, with the enhancement of QDA, the neural network becomes more powerful in detecting multipartite entanglement structures in all possible multi-partitions.

In conclusion, we present a data-augmented deep learning approach for classifying quantum entanglement structures in CV multipartite systems using feasible homodyne measurement statistics. This procedure involves the careful training of a convolutional neural network, where the network is fed with diverse synthetic datasets generated through the QDA method, rooted in fundamental physical principles. The QDA method can be adopted to more multipartite scenarios by leveraging the invariance of target quantum properties under specific operations, which are analogous to the concept of free operations in quantum resource theory. This suggests that insights from quantum resource theory could potentially guide the further development of QDA strategies. With the support of QDA method, the neural network not only captures the underlying entanglement features but also becomes a powerful tool for practical quantum information processing tasks, even when data acquisition cost is exorbitant.

Acknowledgments—This work was supported by the National Natural Science Foundation of China (No. 12125402, No. 12350006, No. 12474256, and No. 12405022), the Innovation Program for Quantum Science and Technology (No. 2021ZD0301500), and Beijing Natural Science Foundation (Grant No. Z240007).

* These authors contributed equally to this work.

† xiangy.phy@pku.edu.cn

‡ qiongyihe@pku.edu.cn

- [1] S. Lohani, B. T. Kirby, M. Brodsky, O. Danaci, and R. T. Glasser, Machine learning assisted quantum state estimation, *Mach. Learn.: Sci. Technol.* **1**, 035007 (2020).
 [2] S. Ahmed, C. Sánchez Muñoz, F. Nori, and A. F. Kockum, Quantum state tomography with conditional generative adversarial networks, *Phys. Rev. Lett.* **127**, 140502 (2021).

- [3] S. Ahmed, C. Sánchez Muñoz, F. Nori, and A. F. Kockum, Classification and reconstruction of optical quantum states with deep neural networks, *Phys. Rev. Res.* **3**, 033278 (2021).
 [4] V. Cimini, M. Barbieri, N. Treps, M. Walschaers, and V. Parigi, Neural networks for detecting multimode Wigner negativity, *Phys. Rev. Lett.* **125**, 160504 (2020).
 [5] Y. Zhu, Y.-D. Wu, G. Bai, D.-S. Wang, Y. Wang, and G. Chiribella, Flexible learning of quantum states with generative query neural networks, *Nat. Commun.* **13**, 6222 (2022).
 [6] V. Gebhart, R. Santagati, A. A. Gentile, E. M. Gauger, D. Craig, N. Ares, L. Banchi, F. Marquardt, L. Pezzè, and C. Bonato, Learning quantum systems, *Nat. Rev. Phys.* **5**, 141 (2023).
 [7] V. V. Sivak, A. Eickbusch, H. Liu, B. Royer, I. Tsioutsios, and M. H. Devoret, Model-free quantum control with reinforcement learning, *Phys. Rev. X* **12**, 011059 (2022).
 [8] Y.-D. Wu, Y. Zhu, G. Bai, Y. Wang, and G. Chiribella, Quantum similarity testing with convolutional neural networks, *Phys. Rev. Lett.* **130**, 210601 (2023).
 [9] X. Gao, M. Isoard, F. Sun, C. E. Lopetegui, Y. Xiang, V. Parigi, Q. He, and M. Walschaers, Correlation-pattern-based continuous variable entanglement detection through neural networks, *Phys. Rev. Lett.* **132**, 220202 (2024).
 [10] J. Brehmer, K. Cranmer, G. Louppe, and J. Pavez, Constraining effective field theories with machine learning, *Phys. Rev. Lett.* **121**, 111801 (2018).
 [11] J. Collins, K. Howe, and B. Nachman, Anomaly detection for resonant new physics with machine learning, *Phys. Rev. Lett.* **121**, 241803 (2018).
 [12] R. Iten, T. Metger, H. Wilming, L. del Rio, and R. Renner, Discovering physical concepts with neural networks, *Phys. Rev. Lett.* **124**, 010508 (2020).
 [13] G. Karagiorgi, G. Kasieczka, S. Kravitz, B. Nachman, and D. Shih, Machine learning in the search for new fundamental physics, *Nat. Rev. Phys.* **4**, 399 (2022).
 [14] A. Jain, H. Patel, L. Nagalapatti, N. Gupta, S. Mehta, S. Guttula, S. Mujumdar, S. Afzal, R. Sharma Mittal, and V. Munigala, Overview and importance of data quality for machine learning tasks, in *Proceedings of the 26th ACM SIGKDD International Conference on Knowledge Discovery & Data Mining*, KDD '20 (Association for Computing Machinery, New York, NY, USA, 2020) p. 3561–3562.
 [15] N. Gupta, S. Mujumdar, H. Patel, S. Masuda, N. Panwar, S. Bandyopadhyay, S. Mehta, S. Guttula, S. Afzal, R. Sharma Mittal, and V. Munigala, Data quality for machine learning tasks, in *Proceedings of the 27th ACM SIGKDD Conference on Knowledge Discovery & Data Mining*, KDD '21 (Association for Computing Machinery, New York, NY, USA, 2021) p. 4040–4041.
 [16] Y. Gong, G. Liu, Y. Xue, R. Li, and L. Meng, A survey on dataset quality in machine learning, *Inform. Software Tech.* **162**, 107268 (2023).
 [17] L. Amico, R. Fazio, A. Osterloh, and V. Vedral, Entanglement in many-body systems, *Rev. Mod. Phys.* **80**, 517 (2008).
 [18] R. Horodecki, P. Horodecki, M. Horodecki, and K. Horodecki, Quantum entanglement, *Rev. Mod. Phys.* **81**, 865 (2009).
 [19] O. Gühne and G. Tóth, Entanglement detection, *Physics Reports* **474**, 1 (2009).

- [20] J. Sperling and W. Vogel, Multipartite entanglement witnesses, *Phys. Rev. Lett.* **111**, 110503 (2013).
- [21] J. Gray, L. Banchi, A. Bayat, and S. Bose, Machine-Learning-Assisted Many-Body Entanglement Measurement, *Phys. Rev. Lett.* **121**, 150503 (2018).
- [22] C. Chen, C. Ren, H. Lin, and H. Lu, Entanglement structure detection via machine learning, *Quantum Sci. Technol.* **6**, 035017 (2021).
- [23] Y. Chen, Y. Pan, G. Zhang, and S. Cheng, Detecting quantum entanglement with unsupervised learning, *Quantum Sci. Technol.* **7**, 015005 (2022).
- [24] Z. Chen, X. Lin, and Z. Wei, Certifying unknown genuine multipartite entanglement by neural networks, *Quantum Sci. and Technol.* **8**, 035029 (2023).
- [25] Y. S. Teo, H. Zhu, B.-G. Englert, J. Řeháček, and Z. c. v. Hradil, Quantum-state reconstruction by maximizing likelihood and entropy, *Phys. Rev. Lett.* **107**, 020404 (2011).
- [26] S. L. Braunstein and P. van Loock, Quantum information with continuous variables, *Rev. Mod. Phys.* **77**, 513 (2005).
- [27] A. I. Lvovsky and M. G. Raymer, Continuous-variable optical quantum-state tomography, *Rev. Mod. Phys.* **81**, 299 (2009).
- [28] E. Chitambar and G. Gour, Quantum resource theories, *Rev. Mod. Phys.* **91**, 025001 (2019).
- [29] M. Gessner, L. Pezzè, and A. Smerzi, Entanglement and squeezing in continuous-variable systems, *Quantum* **1**, 17 (2017).
- [30] U. Chabaud, D. Markham, and F. Grosshans, Stellar representation of non-Gaussian quantum states, *Phys. Rev. Lett.* **124**, 063605 (2020).
- [31] U. Chabaud, G. Ferrini, F. Grosshans, and D. Markham, Classical simulation of Gaussian quantum circuits with non-Gaussian input states, *Phys. Rev. Res.* **3**, 033018 (2021).
- [32] U. Chabaud and S. Mehraban, Holomorphic representation of quantum computations, *Quantum* **6**, 831 (2022).
- [33] M. Eaton, C. González-Arciniegas, R. N. Alexander, N. C. Menicucci, and O. Pfister, Measurement-based generation and preservation of cat and grid states within a continuous-variable cluster state, *Quantum* **6**, 769 (2022).
- [34] M. Tian, X. Gao, B. Jing, F.-X. Sun, M. Fadel, and Q. He, Characterization of multipartite non-Gaussian entanglement structure, arXiv:2408.12554 .
- [35] Supplementary Material for all the detailed calculations in the main text. It includes additional Ref. [36].
- [36] G. S. Agarwal, *Quantum optics* (Cambridge University Press, 2012).
- [37] R. Yamashita, M. Nishio, R. K. G. Do, and K. Togashi, Convolutional neural networks: An overview and application in radiology, *Insights into Imaging* **9**, 611 (2018).
- [38] U. Chabaud and M. Walschaers, Resources for bosonic quantum computational advantage, *Phys. Rev. Lett.* **130**, 090602 (2023).
- [39] C. Shorten and T. M. Khoshgoftaar, A survey on Image Data Augmentation for Deep Learning, *Journal of Big Data* **6**, 60 (2019).
- [40] C. Khosla and B. S. Saini, Enhancing performance of deep learning models with different data augmentation techniques: A survey, in *2020 International Conference on Intelligent Engineering and Management (ICIEM)* (2020) pp. 79–85.